

# Real-time Dissection and Forecast of Infection Dynamics during a Pandemic

Steven Schulz<sup>a,\*</sup>, Richard Pastor<sup>a</sup>, Cenk Koyuncuoglu<sup>a</sup>, Forrest W. Crawford<sup>b,c,d,e</sup>, Detlef Zernick<sup>a</sup>, André Karch<sup>f</sup>, and Sten Rüdiger<sup>a</sup>

<sup>a</sup>*Machine Learning and Health Unit, Department of Engineering, NET CHECK GmbH, Berlin, Germany*

<sup>b</sup>*Department of Biostatistics, Yale School of Public Health, New Haven, CT, USA*

<sup>c</sup>*Department of Statistics and Data Science, Yale University, New Haven, CT, USA*

<sup>d</sup>*Department of Ecology and Evolutionary Biology, Yale University, New Haven, CT, USA*

<sup>e</sup>*Yale School of Management, New Haven, CT, USA*

<sup>f</sup>*Institute of Epidemiology and Social Medicine, Westfälische Wilhelms-Universität Münster, Münster, Germany*

---

## Abstract

Pandemic preparedness requires institutions, including public health authorities and governments, to detect, survey and control outbreaks. To maintain an accurate, quantitative and up-to-date picture of an epidemic crisis is key. For SARS-CoV-2, this was mostly achieved by ascertaining incidence numbers and the effective reproductive number ( $R_{\text{eff}}$ ), which counts how many people an infected person is likely to infect on average. These numbers give strong hints on past infection dynamics in a population but fail to clearly characterize current and future dynamics as well as potential effects of pharmaceutical and non-pharmaceutical interventions. We show that, by using and combining infection surveillance and population-scale contact statistics, we can obtain a better understanding of the drivers of epidemic waves and the effectiveness of interventions. This approach can provide a real-time picture, thus saving not only many lives by quickly allowing adaptation of the health policies but also alleviating economic and other burdens if an intervention proves ineffective. We factorize  $R_{\text{eff}}$  into contacts and relative transmissibility: Both signals can be used, individually and combined, to identify driving forces of an epidemic, monitoring and assessing interventions, as well as projecting an epidemic's future trajectory. Using data for SARS-CoV-2 and Influenza from 2019 onward in Germany, we provide evidence for the usefulness of our approach. In particular, we find that the effects from physical distancing and lockdowns as well as vaccination campaigns are dominant.

---

## 1. Introduction

Infectious diseases represent serious threats to an ever increasingly connected humankind, on par with e.g. natural disasters and infrastructure failures. Epidemic preparedness – the ability to predict and mitigate future epidemic outbreaks – has thus risen to one of the most pressing challenges in modern societies and recently focused a wealth of

research efforts building on a variety of data [1] in response to awareness elicited by the SARS-CoV-2 pandemic [2].

Epidemic dynamics are shaped at the crossroads of human and viral driving forces: a pathogen's reproductive cycle, defining its relative transmission rate upon physical proximity between individuals with full or partial susceptibility, as well as human behaviour, via the frequency of transmission-prone contacts between individuals itself [3]. Critical events such as the emergence of fitter mutants or

---

\*Corresponding author: [steven.schulz@netcheck.de](mailto:steven.schulz@netcheck.de).

collective shifts in human activity patterns set the pace for new epidemic waves. Real-time monitoring of these forces during an epidemic, whether it is fueled mostly by increased contact levels or changes in relative transmissibility, is of paramount value for epidemic forecasting as well as the ability to set up informed, targeted mitigation strategies and estimating the effects of (non-)pharmaceutical health policies [4].

Using SARS-CoV-2 and Influenza as key examples of airborne transmissible contagions, we showcase monitoring and forecast tools for epidemic crises centered around a crowdsourcing-based, real-time method to assess levels of physical proximity in a population using GPS location information, the Contact Index  $CX$  [5]. We show that diverging trends between contact levels and independently recorded infection surveillance are indicators of altered relative viral transmissibility. Using 2020-specific data as a baseline for purely contact-driven SARS-CoV-2 epidemics, all observed transition points are explained by the onset of key immune escape variants (alpha, delta, omicron). The resulting dual evolution, Contact Index  $CX$  and relative transmissibility  $T$ , provides a highly transparent and timely picture of ongoing epidemics, including the possibility to identify likely driving forces in future epidemic waves.

## 2. Materials and Methods

### 2.1. Contact metrics relevant for epidemics

Contact networks are a representation of human interactions [6] with immediate implications for the spread of contagions in a population [7, 8]. Nodes represent individuals and edges are drawn between pairs of nodes in the event of contact between them (Figure S3(a)). A contagion can propagate through a population along paths following the links of the network.

Intuitively, transmission levels scale with the average number of links per node  $\langle k \rangle =$

$\sum_{k \geq 0} kP(k) = 2L/N$  [3], where  $P(k)$  is the distribution of these numbers across a network and  $N$  ( $L$ ) is the number of nodes (links). Beyond this local property, more global topological network features – how contacts are collectively configured across the network – do also affect the course of epidemics [3] by fueling and constraining the number of available paths. Groundbreaking epidemiological and network-theoretical work established that the effective reproduction number  $R_{\text{eff}}$ , quantifying epidemic spreading, scales with  $\frac{\langle k^2 \rangle}{\langle k \rangle}$  [3, 9, 10, 11, 12], i.e. the presence of very social nodes (superspreaders) with outstanding  $k$  mediate enhanced propagation. Typical social networks are very inhomogeneous in terms of social activity, with outstanding community structure and few individuals responsible for most contacts [9]. The pivotal role of the second moment  $\langle k^2 \rangle = \sum_{k \geq 0} k^2 P(k)$  is intuited by the *friendship paradox* [13]: An individual’s friends are on average more social than oneself; in other words, the number of next-nearest neighbors  $\langle k^2 \rangle$  in the network exceeds the expectation  $\langle k \rangle^2$  from the number of nearest neighbors, a mere consequence of non-zero variance in  $P(k)$ :  $\langle k^2 \rangle - \langle k \rangle^2 > 0$ .

### 2.2. Assessing contact levels in real-world networks

The contact network relevant to transmission of airborne viruses such as Influenza and SARS-CoV-2 arises from physical proximity between individuals. Compared to (virtual) social networks, such real-world networks are expected to have distinct properties, as they are constrained by geography and physical distance, but are also tremendously more difficult to track at the population scale. Coarse contact and mixing patterns in real-world networks have been inferred using limited data gathered from surveys [14, 15] or viral phylogeny [16]. Locally confined real-world networks, such as on cruise ships [17], school campuses [18] or within towns [19] have been measured using Bluetooth communication between nearby mobile devices.

We use a previously developed approach to probe population-scale real-world contact networks based on crowdsourced datasets of GPS locations [20, 5] to measure the Contact Index  $CX = \frac{\langle k^2 \rangle}{\langle k \rangle}$  as a statistical measure of contact levels relevant for epidemics [5]. The crowdsourcing data is collected in near real-time via opt-in from each of an anonymized panel of 1 million mobile app users (roughly 1% of Germany’s population) and consists of  $\approx 100$  daily samples per device tagged with time and GPS location information. It allows us to reconstruct samples of the actual contact network realized in the population: Contacts (links) are drawn between devices (nodes) co-located in space and time (Supp Mat S1).

### 2.3. Network sampling correction

The incomplete nature of such crowdsourced data represents a major challenge: Contacts from uninvolved or inactive devices are not captured, giving rise to missing nodes and links in the network. This aspect of our data can be crafted into a network sampling framework [21, 22] in which nodes and edges are randomly removed with probabilities  $p$  and  $q$ , respectively (Figure S3(a,b) and Supp Mat S2). These sampling parameters also change over time, mostly in response to software updates and app usage, and are heterogeneous in space. Our improved mathematical modeling based on Horvitz-Thompson theory disentangles actual changes in contact levels from signals unrelated to the users’ contact behaviour, thus achieving persistent and comparable results across the full time span since the beginning of measurement in 2019 (Supp Mat S2 and Supp Mat S3).

Importantly, abstractions of contact networks exist in two distinct flavours: weighted versus unweighted [23]. Links may be endowed with weights  $w_{ij} \in \{0, 1, 2, \dots\}$  representing the duration or multiplicity of contact between individuals  $i$  and  $j$  [24] or simply indicate the presence or absence of contact  $a_{ij} = \text{sgn}(w_{ij}) \in \{0, 1\}$  (Figure S3(c)). In

the epidemiological context, we assume that network topology, represented by  $a_{ij}$ , is more important than the recurrence of contacts between the same individuals: For instance, the (statistical) contribution to viral spread from a cluster of short contacts at a crowded event would outpace a lengthy contact between an isolated couple while in lockdown. We thus focus on unweighted networks and exclude contact duration in our analyses other than in the fact that short contacts are unlikely to be recorded during the random sampling inherent to the crowdsourcing method.

However, network sampling destroys topological information about underlying complete networks (Figure S3(c)); the success of Horvitz-Thompson theory [21] to establish a connection between original and sample networks relies in the use of weighted links. To establish the same connection for unweighted networks, we devised a Bayesian framework which encodes missing topological information as a prior weight distribution  $P(w|w > 0)$  (Supp Mat S2). We find that available complete real-world networks in various contexts [17, 18, 19] appear to show strikingly similar weight distributions (Figure S3(d)), which suggests a universal shape of  $P(w|w > 0)$  also applicable to our problem. These distributions are consistent with power laws with small exponents [25, 26], a repeatedly demonstrated feature of complex networks [27] and beyond [28]. Yet, we do not imply that power laws are the true mechanism behind network weights, as a variety of other distribution classes are easily confounded with power laws [28, 29, 30].

## 3. Results

### 3.1. Evolution of $CX$ since 2019

By means of our refined correction method for network sampling effects, we achieve a consistent measurement of contact levels since the beginning of crowdsourcing in 2019, despite the time-dependent sampling. That is, we cover the prelude

181 and entire course of the SARS-CoV-2 epidemic in  
182 Germany (Figure 1(a)). The gap in February 2020  
183 is explained by missing data due to the rollout of a  
184 major crowdsourcing software update.

185 Holiday season comes along with reduced  $CX$  un-  
186 der normal conditions, as shown by the Fall and  
187 Christmas breaks in 2019, thus showing a reduction  
188 of transmission-prone contacts. The onset of the  
189 first SARS-CoV-2 wave in March 2020 induced an  
190 unequivocally more pronounced drop in  $CX$ , prob-  
191 ably explained by a more systematic cessation of  
192 super-spreading activities.

193 Since onset of the SARS-CoV-2 pandemic,  
194 changes in contact behaviour as reflected by  $CX$   
195 underwent several periods of spiking (partial or  
196 complete deregulation of mass events in fall 2020,  
197 fall 2021 and spring 2022) and damping (winter  
198 wave 2020, emergence of the omicron variant in  
199 late 2021). Overall, a similar evolution is observed  
200 between  $CX$  and the rigor of SARS-CoV-2-related  
201 policy as measured by the Government-Response  
202 Index [31] (Figure S1(a)), thus indicating broad  
203 awareness of the situation at the population and  
204 governance levels albeit no causal link shall be im-  
205 plied.

206 Interestingly, recent  $CX$  values have not yet re-  
207 turned to pre-pandemic levels by a factor of 2 to 3,  
208 despite a return to no contact-related restrictions  
209 in 2022. This suggests the existence of a hystere-  
210 sis effect in addition to the fast response of  $CX$   
211 discussed above: The collective behaviour has not  
212 returned to its unperturbed state in response to re-  
213 laxed conditions, possibly as a result of continued  
214 broad perception of disease risk [32, 33].

215 From a dimensional viewpoint,  $CX$  represents  
216 an average number of (next-nearest) contacts per  
217 (nearest) contact: Comparing values of  $CX$  across  
218 areas with vastly different population densities  
219 within Germany supports our expectation that  $CX$   
220 scales (non-linearly) with the absolute propensity  
221 of physical proximity between individuals (Fig-

222 ure S4(d) and Supp Mat S3).

### 223 3.2. Deciphering epidemic forces: contacts vs. rel- 224 ative transmissibility

225 In 2020, SARS-CoV-2 epidemic trends were pri-  
226 marily driven by trends in contact levels, as both  
227 immune escape variants and vaccines were not yet  
228 relevant and relative SARS-CoV-2 transmissibility  
229 – its intrinsic transmission probability per contact  
230 – was thus constant (Figure 1(b)): Official daily  
231 now-cast reproduction numbers  $R_{\text{eff}}$ , independently  
232 recorded from national infection surveillance [34],  
233 correlate well with daily  $CX$ , but  $CX$  shows a  
234 time lead of approximately 2 – 3 weeks over  $R_{\text{eff}}$   
235 (Figure S1(a, right inset)) [5], explained by incu-  
236 bation time as well as testing and reporting de-  
237 lays. This underlines the predictive character of  
238 real-time contact metrics for wild-type dominated  
239 epidemics [20]. Since then, the correlation between  
240  $R_{\text{eff}}$  and  $CX$  has repeatedly changed, with the re-  
241 sulting signal quantifying shifts in relative transmis-  
242 sibility accountable to key epidemic changes other  
243 than contacts.

244 The effective reproduction number  $R_{\text{eff}}$  is defined  
245 by  $R_{\text{eff}} = \langle k \rangle \cdot U \cdot \tau$ , where  $\langle k \rangle$  denotes the contact  
246 number per day,  $U$  the probability of transmission  
247 per contact, and  $\tau$  the mean duration of infectivity  
248 in days. Both  $U$  and  $\tau$  are determined by physio-  
249 logical processes involved in transmission and, to-  
250 gether, define the intrinsic transmission efficiency  
251 (per contact)  $T = U \cdot \tau$ .

252 Furthermore, as we assume  $CX = \frac{\langle k^2 \rangle}{\langle k \rangle}$   
253 replaces  $\langle k \rangle$ , we replace the definition by  
254  $R_{\text{eff}} = (a + b \cdot CX) \cdot T$ . A linear relationship of  
255 this form between  $CX$  and  $R_{\text{eff}}$  is motivated by our  
256 findings in 2020. We use values for  $a$  and  $b$  obtained  
257 from a linear regression between  $CX$  and wild-type  
258  $R_{\text{eff}}$  data at the optimal time delay of  $\Delta t = 16$  days  
259 (Figure S1(a, left inset) and Supp Mat S4). Upon  
260 interpreting  $R_{\text{WT}}(CX) \equiv a + b \cdot CX$  as the wild-type

261 specific reproduction number, we have that

$$R_{\text{eff}} = R_{\text{WT}}(CX) \cdot T, \quad (1)$$

262 where  $T$  represents relative transmissibility with re-  
263 spect to wild-type in a fully susceptible population  
264 ( $T_{\text{WT}} = 1$ ). Note that, in contrast to now-cast data,  
265 Eq. (1) assigns reproduction numbers to the day of  
266 contact/infection.

267 From independently recorded values for  $R_{\text{eff}}$  and  
268  $CX$ , we can determine the relative transmissi-  
269 bility of the contagion by factoring out contact-  
270 related contributions from overall infection dynam-  
271 ics as  $T = \frac{R_{\text{eff}}}{R_{\text{WT}}(CX)}$  for any given day. We ex-  
272 pect network-wide propagation of transmissibility-  
273 related information to be slow compared to network  
274 dynamics itself and, thus,  $T$  to undergo evolution  
275 on longer timescales. We interpret fast signal in  
276  $T$  as random fluctuations from the measurement of  
277  $R_{\text{eff}}$  and capture actual trends by  $\langle T \rangle$ , centered av-  
278 erages over sliding time windows of 2 months (Supp  
279 Mat S4).

### 280 3.3. Epidemic evolution of relative SARS-CoV-2 281 transmissibility

282 The evolution of relative SARS-CoV-2 transmis-  
283 sibility  $\langle T \rangle$  is shown in Figure 1(b). This time se-  
284 ries reenacts the various phases of the SARS-CoV-2  
285 pandemic:

286 Relative SARS-CoV-2 transmissibility  $\langle T \rangle$  is ap-  
287 proximately equal to unity throughout 2020, an  
288 initial period purely driven by unperturbed wild-  
289 type epidemics that we used to “calibrate”  $CX$  and  
290  $R_{\text{eff}}$  which evolve on shorter timescales. It sub-  
291 sequently follows a tug-of-war pattern shaped by  
292 alternating epidemic forces beyond contacts: im-  
293 mune escape variants and development of popula-  
294 tion immunity through infection and vaccination.  
295 Three waves of increased relative transmissibility  
296 are explained by the takeover of fitter virus lin-  
297 eages (Figure 1(b)), specifically alpha (spring 2021),  
298 delta (summer 2021) and omicron BA.1/BA.2 (win-

299 ter 2021/22). We hypothesize that subsequent re-  
300 laxation of  $\langle T \rangle$  after each wave may be attributed to  
301 natural immunity, while the superposed long-term  
302 downward trend may be explained by the additional  
303 immunity acquisition through (initial and booster)  
304 vaccination campaigns. Interestingly, the effect of  
305 omicron BA.4/BA.5 takeover in summer 2022 on  
306  $\langle T \rangle$  is nowhere close to those of previous variants.

307 Comparing correlations with different param-  
308 eters rules out the possibility that the measured  $\langle T \rangle$   
309 is shaped by factors confounding the reproduction  
310 numbers or  $CX$  values (Figure S1(b,c) and Supp  
311 Mat S4). These possible confounders include viral  
312 prevalence,  $CX$  itself through higher-order effects  
313 from network sampling not captured by our mod-  
314 eling and other topological network features (such  
315 as clustering, small-world properties) as well as  $R_{\text{eff}}$   
316 itself through changes in testing strategies and sys-  
317 tematic under-reporting of infections [35]. For in-  
318 stance, testing individuals indiscriminately versus  
319 focusing test capacities on suspected infection cases  
320 may lead to incomparable snapshots of ongoing in-  
321 fection dynamics. Overall, strong positive correla-  
322 tion is exclusively observed between  $\langle T \rangle$  and variant  
323 dynamics (Figure S1(b,c)) [36]. In this analysis, we  
324 use test positivity [37] and results from local preva-  
325 lence studies [38] as proxies for overall prevalence.  
326 Also, we neglect possible effects from network sam-  
327 pling on different topological measures [39, 40], but  
328 we expect trends to be conserved as long as the  
329 sampling process remains unchanged.

330 We note the absence of seasonal oscillations in  
331  $\langle T \rangle$  as well as clear signatures of mask mandates  
332 (in effect across many social contexts between April  
333 2020 and April 2022). A seasonal oscillation in  $\langle T \rangle$ ,  
334 larger values in winter and smaller values in sum-  
335 mer, might be expected from the shift of human ac-  
336 tivity between in- and outdoor settings. Also, pre-  
337 vious research established the effectiveness of mask  
338 usage at reducing transmission of respiratory dis-  
339 eases (reviewed in [41]). Overall, our results sug-

340 gest that, at least in the epidemic stage of SARS-  
 341 CoV-2, infection rates were predominantly driven  
 342 by the strong variability in contacts as well as the  
 343 repeated emergence of more transmissible variants,  
 344 in line with previous findings [42, 43, 44].

### 345 3.4. Forecast of infection level and trend changes

346 The challenge of epidemic forecast consists in the  
 347 accurate prediction of current and future reproduc-  
 348 tion numbers  $R_{\text{eff}}$ . Using the rationale that trends  
 349 in infection levels carry the combined signature of  
 350 trends in contact and relative transmissibility lev-  
 351 els, we propose to construct predictions according  
 352 to

$$R_{\text{true}}(t) = R_{\text{WT}}(CX(t)) \cdot \langle T(t) \rangle, \quad (2)$$

353 where  $R_{\text{true}}$  is assigned to the projected day of con-  
 354 tact/infection. The key difference to Eq. (1) is the  
 355 use of  $\langle T \rangle$  which eliminates noise from reproduc-  
 356 tion numbers. Importantly, we therefore expect  
 357 that our prediction  $R_{\text{true}}$  represents actual epidemic  
 358 trends (ground truth) more accurately than epi-  
 359 demic surveillance ( $R_{\text{eff}}$ ).

360 Figure 1(c) shows  $R_{\text{true}}$  together with data from  
 361 infection surveillance, both plotted with respect to  
 362 their date of recording (assuming real-time  $CX$   
 363 measurement). This shows how our prediction  
 364 overall anticipates current epidemic trends that  
 365 are observed via infection surveillance only about  
 366  $\Delta t = 2 - 3$  weeks later. Thus, we propose to use  
 367 our method as a tool for real-time infection surveil-  
 368 lance.

369 To extend forecasts beyond this horizon and pre-  
 370 dict future reproduction numbers,  $CX$  and  $\langle T \rangle$   
 371 themselves need to be projected beyond latest data.  
 372 For several choices of the current day  $t_0$ , Figure 2(a)  
 373 showcases forecasts ( $R_{\text{pred}}$ ) where  $CX$  and  $\langle T \rangle$  are  
 374 continued beyond the last days of available data  
 375 ( $t_0$  and  $t_0 - \Delta t$ , respectively) using autoregressive  
 376 integrated moving average (ARIMA) models prior  
 377 to applying Eq. (2) (Supp Mat S5). These fore-

378 casts outperform a null forecast based on a mere  
 379 ARIMA-type continuation of infection surveillance  
 380 data ( $R_{\text{eff}}$ ), as shown by narrower distributions of  
 381 residuals ( $R_{\text{pred}} - R_{\text{true}}$ ) across all choices of  $t_0$  (Fig-  
 382 ure 2(a)). Furthermore, we highlight the broad ap-  
 383 plicability of our method to airborne infectious dis-  
 384 eases by performing an identical forecast analysis  
 385 for Influenza (Figure S2(a)), using coarser infection  
 386 surveillance data [45] and presuming a similar rela-  
 387 tionship between  $R_{\text{eff}}$  and  $CX$  as for SARS-CoV-2  
 388 (Supp Mat S5).

389 Most importantly, trend changes in epidemic  
 390 driving forces such as  $\langle T \rangle$  and  $CX$  are indicators of  
 391 new phases in an epidemic. Timely detection of new  
 392 trends in these time series, e.g. using anomaly de-  
 393 tection methods, can provide valuable information  
 394 to estimate the risk of upcoming epidemic waves  
 395 and to predict their nature – whether dynamics is  
 396 fueled by contacts or increased transmission effi-  
 397 ciency. Such trend detection is potentially easier  
 398 to achieve but equally informative than the abil-  
 399 ity to accurately predict infection surveillance. The  
 400 onset of rising trends could shape decision-making  
 401 with regard to the effectiveness of health policies,  
 402 e.g. pharmaceutical and non-pharmaceutical in-  
 403 terventions for rising  $\langle T \rangle$  and  $CX$ , respectively.  
 404 Figures 2(b) and S2(b) highlight rising and falling  
 405 trends in both  $CX$  and  $T$  for SARS-CoV-2 and In-  
 406 fluenza, respectively, akin to trends in stock prices.  
 407 For SARS-CoV-2, trend changes are timely indica-  
 408 tors of all major escape variant- and contact-driven  
 409 epidemic turning points (Figure 2(b)). Unlike for  
 410 SARS-CoV-2 in its epidemic stage, major upheavals  
 411 in relative transmissibility for Influenza are limited  
 412 to seasonality, with the notable exception of 2020,  
 413 presumably reflecting its endemic dynamics (Fig-  
 414 ure S2(b)).

## 415 4. Conclusion

416 We presented a simple, yet insightful quantitative  
 417 method for a data-driven decomposition of overall

418 epidemic dynamics into contact-related and trans- 459  
419 mission efficiency-related contributions. It relies on 460  
420 both the availability of infection surveillance data 461  
421 as well as crowdsourced GPS location data to detect 462  
422 and quantify physical proximity between suscepti- 463  
423 ble individuals. Its appeal resides in the merely 464  
424 bivariate yet highly informative projection of epi- 465  
425 demics paving the way towards timely identifica- 466  
426 tion of driving forces in an ongoing epidemic – hu- 467  
427 man versus viral factors – and possibly effective 468  
428 mitigation strategies – pharmaceutical versus non- 469  
429 pharmaceutical.

430 The approach can be used for epidemic forecast 471  
431 in multiple ways. Recent and projected future val- 472  
432 ues of  $CX$  and  $\langle T \rangle$  can be used for short-term 473  
433 ( $2 - 3$  weeks) and long-term prediction of infection 474  
434 or reproduction numbers, thus taking our previ- 475  
435 ously described short-term forecast further [5]. Yet, 476  
436 a timely detection of trend changes could reliably 477  
437 forecast upcoming waves and their nature without 478  
438 the necessity to accurately predict infection surveil- 479  
439 lance data. These tools can lead towards a more 480  
440 strategic approach to epidemic mitigation and po- 481  
441 tentially save lives by reducing the spread of deadly 482  
442 diseases.

443 Results from the presumably most systematically 484  
444 tracked epidemic to date, SARS-CoV-2, draw the 485  
445 picture of co-evolution within the virus-host rela- 486  
446 tion: Increasing immunity levels in the host pop- 487  
447 ulation alternate with step-wise adaptation of the 488  
448 virus through immune-escape variants. Other fre- 489  
449 quently discussed factors, including mask policies 490  
450 and seasonality, are presumably still below the cur- 491  
451 rent statistical resolution of our method, defined by 492  
452 the sampling noise in the  $CX$  and  $R_{\text{eff}}$  time series.  
453 Moreover, a larger impact of seasonal variation is  
454 expected in the endemic phase of SARS-CoV-2 [46].

455 Our method is broadly applicable to airborne 494  
456 contagions beyond SARS-CoV-2, but depends on 495  
457 the availability of infection surveillance and crowd- 496  
458 sourcing strategies that remain persistent over ex- 497

tended amounts of time. Changes in testing strat-  
egy can lead to signal and biases unrelated to un-  
derlying epidemic driving forces [35]. More cru-  
cially, systematic infection surveillance is not im-  
plemented beyond the case of SARS-CoV-2. We  
illustrated a framework to correct for the effect  
of varying sampling depth in the contact network.  
Yet, higher-order effects in the signal can occur as  
a result of sampling aspects not captured by our  
mathematical modeling. In order to ensure valid  
prognoses through our method, we advocate for sys-  
tematic and persistent crowdsourcing and infection  
surveillance strategies across a variety of diseases  
with epidemic potential.

Geographical resolution of our forecast method  
is currently limited by the sampling depth, as the  
estimation especially of higher moments of degree  
distributions  $P(k)$  becomes increasingly difficult as  
smaller portions of the network are available. A  
higher spatial resolution of contact and relative  
transmissibility levels, with potential to locate the  
origin of new variants of concern and define locally  
targeted mitigation strategies, can be achieved by  
e.g. increasing the panel of app users.

Our analysis assumes statics, but actual contact  
networks are dynamic in nature [47, 48]: While  
some contacts are frequently repeated (e.g. be-  
tween household members), other contacts are ran-  
domly redrawn on each occasion (e.g. in pub-  
lic transportation), with implications for epidemic  
spread [49, 50]. Our method can be improved by  
analyzing contact data in light of existing models  
of dynamic networks [51, 48].

## 492 Acknowledgment

This work was supported by grants from the  
Federal Government of Germany through the  
Federal Ministry for Economic Affairs and Cli-  
mate Action (BMWK) for the project DAKI-FWS  
(01MK21009A) and the Federal Ministry of Educa-

498 tion and Research (BMBF) for the project Optim-  
499 Agent (031L0299).

## 500 References

501 [1] A. Rodríguez, H. Kamarthi, P. Agarwal, J. Ho, M. Pa-  
502 tel, S. Sapre, B. A. Prakash, Data-centric epidemic  
503 forecasting: A survey, arXiv preprint arXiv:2207.09370  
504 (2022).

505 [2] A. Maxmen, Has covid taught us anything about pan-  
506 demic preparedness?, *Nature* (2021) 332–335.

507 [3] R. Pastor-Satorras, C. Castellano, P. Van Mieghem,  
508 A. Vespignani, Epidemic processes in complex net-  
509 works, *Reviews of modern physics* 87 (3) (2015) 925.

510 [4] T. Alamo, D. G. Reina, P. M. Gata, V. M. Preciado,  
511 G. Giordano, Data-driven methods for present and fu-  
512 ture pandemics: Monitoring, modelling and managing,  
513 *Annual Reviews in Control* 52 (2021) 448–464.

514 [5] S. Rüdiger, S. Konigorski, A. Rakowski, J. A. Edelman,  
515 D. Zernick, A. Thieme, C. Lippert, Predicting the sars-  
516 cov-2 effective reproduction number using bulk contact  
517 data from mobile phones, *Proceedings of the National*  
518 *Academy of Sciences* 118 (31) (2021).

519 [6] M. E. Newman, J. Park, Why social networks are dif-  
520 ferent from other types of networks, *Physical review E*  
521 68 (3) (2003) 036122.

522 [7] M. Keeling, The implications of network structure  
523 for epidemic dynamics, *Theoretical population biology*  
524 67 (1) (2005) 1–8.

525 [8] C. Moore, M. E. Newman, Epidemics and percolation in  
526 small-world networks, *Physical Review E* 61 (5) (2000)  
527 5678.

528 [9] M. Barthélemy, A. Barrat, R. Pastor-Satorras,  
529 A. Vespignani, Dynamical patterns of epidemic out-  
530 breaks in complex heterogeneous networks, *Journal of*  
531 *theoretical biology* 235 (2) (2005) 275–288.

532 [10] Y. Moreno, R. Pastor-Satorras, A. Vespignani, Epi-  
533 demic outbreaks in complex heterogeneous networks,  
534 *The European Physical Journal B-Condensed Matter*  
535 *and Complex Systems* 26 (4) (2002) 521–529.

536 [11] R. M. May, R. M. Anderson, The transmission dynam-  
537 ics of human immunodeficiency virus (hiv), *Philosophical*  
538 *Transactions of the Royal Society of London. B,*  
539 *Biological Sciences* 321 (1207) (1988) 565–607.

540 [12] R. M. May, R. M. Anderson, Commentary transmission  
541 dynamics of hiv infection, *Nature* 326 (137) (1987) 10–  
542 1038.

543 [13] S. L. Feld, Why your friends have more friends than you  
544 do, *American journal of sociology* 96 (6) (1991) 1464–  
545 1477.

546 [14] J. M. Read, K. T. Eames, W. J. Edmunds, Dynamic  
547 social networks and the implications for the spread of

infectious disease, *Journal of The Royal Society Inter-*  
548 *face* 5 (26) (2008) 1001–1007.

- 550 [15] J. Mossong, N. Hens, M. Jit, P. Beutels, K. Auranen,  
551 R. Mikolajczyk, M. Massari, S. Salmaso, G. S. Tomba,  
552 J. Wallinga, et al., Social contacts and mixing pat-  
553 terns relevant to the spread of infectious diseases, *PLoS*  
554 *medicine* 5 (3) (2008) e74.
- 555 [16] G. E. Leventhal, R. Kouyos, T. Stadler, V. Von Wyl,  
556 S. Yerly, J. Böni, C. Cellera, T. Klimkait, H. F.  
557 Günthard, S. Bonhoeffer, Inferring epidemic contact  
558 structure from phylogenetic trees, *PLoS computational*  
559 *biology* 8 (3) (2012) e1002413.
- 560 [17] R. Pung, J. A. Firth, L. G. Spurgin, V. J. Lee, A. J.  
561 Kucharski, Using high-resolution contact networks to  
562 evaluate sars-cov-2 transmission and control in large-  
563 scale multi-day events, *Nature communications* 13 (1)  
564 (2022) 1–11.
- 565 [18] P. Sapiezynski, A. Stopczynski, D. D. Lassen,  
566 S. Lehmann, Interaction data from the copenhagen net-  
567 works study, *Scientific Data* 6 (1) (2019) 1–10.
- 568 [19] S. M. Kissler, P. Klepac, M. Tang, A. J. Conlan, J. R.  
569 Gog, Sparking “the bbc four pandemic”: Leveraging  
570 citizen science and mobile phones to model the spread  
571 of disease, *BioRxiv* (2020) 479154.
- 572 [20] F. W. Crawford, S. A. Jones, M. Cartter, S. G. Dean,  
573 J. L. Warren, Z. R. Li, J. Barbieri, J. Campbell, P. Ken-  
574 ney, T. Valleau, et al., Impact of close interpersonal  
575 contact on covid-19 incidence: Evidence from 1 year  
576 of mobile device data, *Science Advances* 8 (1) (2022)  
577 eabi5499.
- 578 [21] E. D. Kolaczyk, G. Csárdi, *Statistical analysis of net-*  
579 *work data with R*, Vol. 65, Springer, 2014.
- 580 [22] P. Hu, W. C. Lau, A survey and taxonomy of graph  
581 sampling, arXiv preprint arXiv:1308.5865 (2013).
- 582 [23] M. Á. Serrano, M. Boguñá, R. Pastor-Satorras, Corre-  
583 lations in weighted networks, *Physical Review E* 74 (5)  
584 (2006) 055101.
- 585 [24] A. Barrat, M. Barthelemy, R. Pastor-Satorras,  
586 A. Vespignani, The architecture of complex weighted  
587 networks, *Proceedings of the national academy of sci-*  
588 *ences* 101 (11) (2004) 3747–3752.
- 589 [25] H. Ebel, L.-I. Mielsch, S. Bornholdt, Scale-free topol-  
590 ogy of e-mail networks, *Physical review E* 66 (3) (2002)  
591 035103.
- 592 [26] M. E. Newman, Scientific collaboration networks. i. net-  
593 work construction and fundamental results, *Physical re-*  
594 *view E* 64 (1) (2001) 016131.
- 595 [27] R. Guimera, S. Mossa, A. Turtleschi, L. N. Amaral,  
596 The worldwide air transportation network: Anoma-  
597 lous centrality, community structure, and cities’ global  
598 roles, *Proceedings of the National Academy of Sciences*  
599 102 (22) (2005) 7794–7799.



- 600 [28] A. Clauset, C. R. Shalizi, M. E. Newman, Power-law 652  
601 distributions in empirical data, *SIAM review* 51 (4) 653  
602 (2009) 661–703. 654
- 603 [29] J.-D. J. Han, D. Dupuy, N. Bertin, M. E. Cusick, 655  
604 M. Vidal, Effect of sampling on topology predictions 656  
605 of protein-protein interaction networks, *Nature biotechnol-* 657  
606 *ogy* 23 (7) (2005) 839–844. 658
- 607 [30] R. Perline, Strong, weak and false inverse power laws, 659  
608 *Statistical Science* (2005) 68–88. 660
- 609 [31] T. Hale, N. Angrist, R. Goldszmidt, B. Kira, A. Pether- 661  
610 ick, T. Phillips, S. Webster, E. Cameron-Blake, L. Hal- 662  
611 las, S. Majumdar, et al., A global panel database of pan- 663  
612 demic policies (oxford covid-19 government response 664  
613 tracker), *Nature human behaviour* 5 (4) (2021) 529– 665  
614 538. 666
- 615 [32] C. Betsch, S. Eitze, P. Sprengholz, L. Korn, P. Sham- 667  
616 srizi, M. Geiger, E. Sievert, L. Lehrer, M. Jenny, Zusammen- 668  
617 fassung und empfehlungen welle 69 (2022). 669  
618 URL [https://projekte.uni-erfurt.de/cosmo2020/](https://projekte.uni-erfurt.de/cosmo2020/web/summary/69/) 670  
619 [web/summary/69/](https://projekte.uni-erfurt.de/cosmo2020/web/summary/69/) 671
- 620 [33] C. Betsch, L. Wieler, M. Bosnjak, M. Ramharter, 672  
621 V. Stollorz, S. Omer, L. Korn, P. Sprengholz, L. Fel- 673  
622 gendreff, S. Eitze, P. Schmid, Germany covid-19 snap- 674  
623 shot monitoring (cosmo germany): Monitoring knowl- 675  
624 edge, risk perceptions, preventive behaviours, and pub- 676  
625 lic trust in the current coronavirus outbreak in germany 677  
626 (Mar. 2020). doi:10.23668/psycharchives.2776. 678  
627 URL [https://psycharchives.org/index.php/en/](https://psycharchives.org/index.php/en/item/e5acdc65-77e9-4fd4-9cd2-bf6aa2dd5eba) 679  
628 [item/e5acdc65-77e9-4fd4-9cd2-bf6aa2dd5eba](https://psycharchives.org/index.php/en/item/e5acdc65-77e9-4fd4-9cd2-bf6aa2dd5eba) 680
- 629 [34] M. an der Heiden, Sars-cov-2-nowcasting und -r- 681  
630 schaetzung (Jan. 2023). doi:10.5281/zenodo.7571376. 682  
631 URL <https://doi.org/10.5281/zenodo.7571376> 683
- 632 [35] H. Rossman, E. Segal, Nowcasting the spread of sars- 684  
633 cov-2, *Nature microbiology* 7 (1) (2022) 16–17. 685
- 634 [36] R. Koch-Institut. [link]. 686  
635 URL [https://www.rki.de/DE/Content/InfAZ/](https://www.rki.de/DE/Content/InfAZ/N/Neuartiges_Coronavirus/Daten/VOC_VOI/_Tabelle.xlsx?__blob=publicationFile) 687  
636 [N/Neuartiges\\_Coronavirus/Daten/VOC\\_VOI/](https://www.rki.de/DE/Content/InfAZ/N/Neuartiges_Coronavirus/Daten/VOC_VOI/_Tabelle.xlsx?__blob=publicationFile) 688  
637 [\\_Tabelle.xlsx?\\_\\_blob=publicationFile](https://www.rki.de/DE/Content/InfAZ/N/Neuartiges_Coronavirus/Daten/VOC_VOI/_Tabelle.xlsx?__blob=publicationFile) 689
- 638 [37] E. Mathieu, H. Ritchie, L. Rodés-Guirao, C. Appel, 690  
639 C. Giattino, J. Hasell, B. Macdonald, S. Dat- 691  
640 tani, D. Beltekian, E. Ortiz-Ospina, M. Roser, 692  
641 Coronavirus pandemic (covid-19), *Our World in* 693  
642 *Data*<https://ourworldindata.org/coronavirus> (2020). 694
- 643 [38] H. Neuhauser, N. Buttman-Schweiger, J. Fiebig, 695  
644 C. Poethko-Müller, F. Prütz, G. Sarganas Margolis, 696  
645 R. Thamm, M. Zimmermann, Observatorium serolo-  
646 gischer Studien zu SARS-CoV-2 in Deutschland (Sep.  
647 2022). doi:10.5281/zenodo.7043025.  
648 URL <https://doi.org/10.5281/zenodo.7043025>
- 649 [39] J. D. Noh, Percolation transition in networks with  
650 degree-degree correlation, *Physical Review E* 76 (2)  
651 (2007) 026116.
- [40] S. H. Lee, P.-J. Kim, H. Jeong, Statistical properties  
of sampled networks, *Physical review E* 73 (1) (2006)  
016102.
- [41] J. T. Brooks, J. C. Butler, Effectiveness of mask wear-  
ing to control community spread of sars-cov-2, *Jama*  
325 (10) (2021) 998–999.
- [42] F. Balloux, C. Tan, L. Swadling, D. Richard, C. Jenner,  
M. Maini, L. van Dorp, The past, current and future  
epidemiological dynamic of sars-cov-2, *Oxford open im-*  
*munology* 3 (1) (2022) iqac003.
- [43] G. P. Guy Jr, F. C. Lee, G. Sunshine, R. McCord,  
M. Howard-Williams, L. Kompaniyets, C. Dunphy,  
M. Gakh, R. Weber, E. Sauber-Schatz, et al., Asso-  
ciation of state-issued mask mandates and allowing on-  
premises restaurant dining with county-level covid-19  
case and death growth rates—united states, march 1–  
december 31, 2020, *Morbidity and Mortality Weekly*  
*Report* 70 (10) (2021) 350.
- [44] D. K. Chu, E. A. Akl, S. Duda, K. Solo, S. Yaa-  
coub, H. J. Schünemann, A. El-Harakeh, A. Bognanni,  
T. Lotfi, M. Loeb, et al., Physical distancing, face  
masks, and eye protection to prevent person-to-person  
transmission of sars-cov-2 and covid-19: a system-  
atic review and meta-analysis, *The lancet* 395 (10242)  
(2020) 1973–1987.
- [45] R. Koch-Institut, *Survstat@rki* 2.0.  
URL <https://survstat.rki.de/>
- [46] J. P. Townsend, A. D. Lamb, H. B. Hassler, P. Sah,  
A. A. Nishio, C. Nguyen, A. D. Tew, A. P. Galvani,  
A. Dornburg, Projecting the seasonality of endemic  
covid-19, *medRxiv* (2022) 2022–01.
- [47] V. Sekara, A. Stopczynski, S. Lehmann, Fundamental  
structures of dynamic social networks, *Proceedings of*  
*the national academy of sciences* 113 (36) (2016) 9977–  
9982.
- [48] P. Holme, J. Saramäki, Temporal networks, *Physics re-*  
*ports* 519 (3) (2012) 97–125.
- [49] J. Enright, R. R. Kao, Epidemics on dynamic networks,  
*Epidemics* 24 (2018) 88–97.
- [50] E. Valdano, L. Ferreri, C. Poletto, V. Colizza, Analyti-  
cal computation of the epidemic threshold on temporal  
networks, *Physical Review X* 5 (2) (2015) 021005.
- [51] X. Zhang, C. Moore, M. E. Newman, Random graph  
models for dynamic networks, *The European Physical*  
*Journal B* 90 (10) (2017) 1–14.

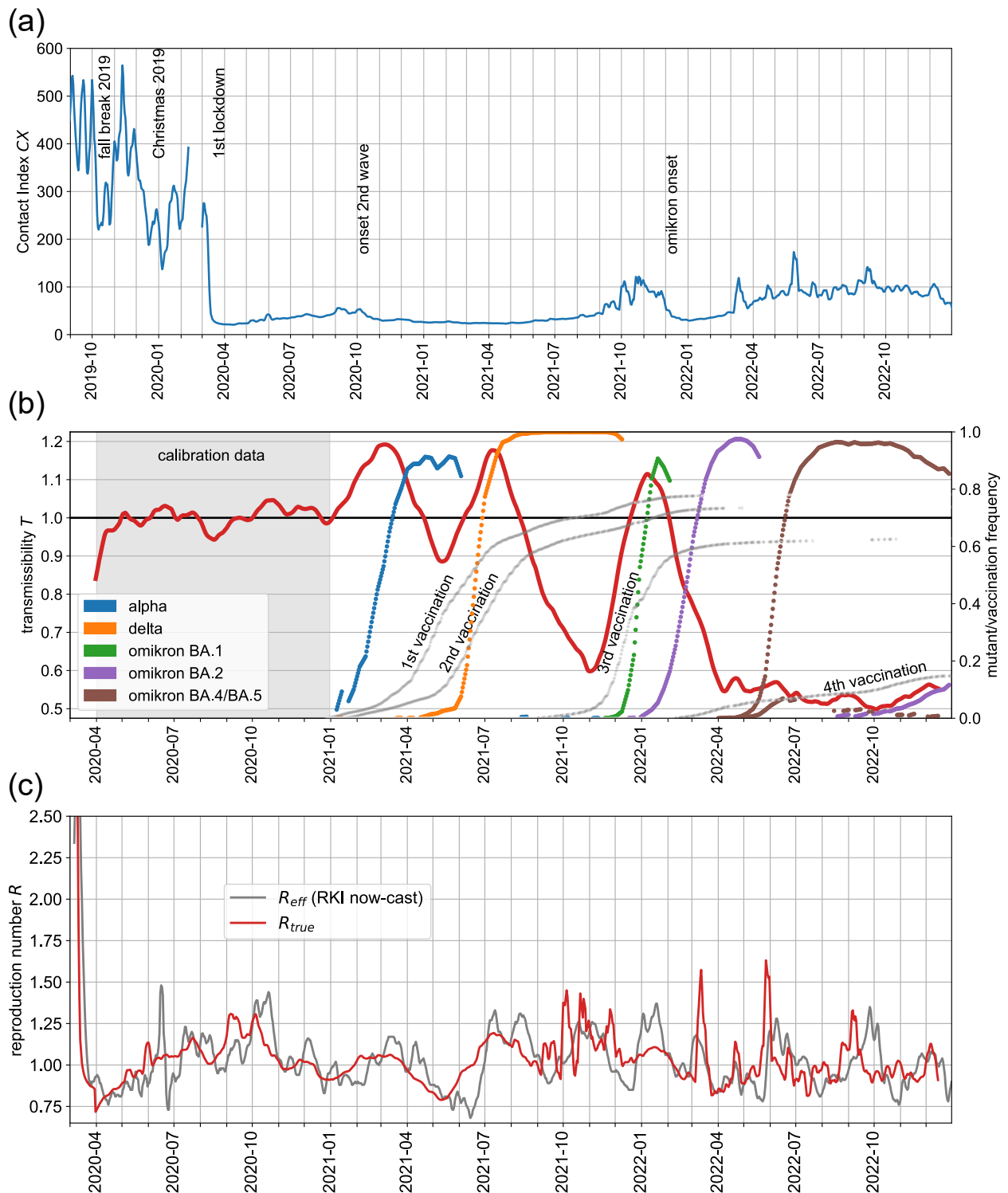


**Figure 1: Real-time observation of driving forces in SARS-CoV-2 epidemics: contact levels and relative transmissibility.** (a) Evolution of the Contact Index  $CX = \langle k^2 \rangle / \langle k \rangle$  in Germany over the course of > 3 years (2019-2022), carrying the signature of various collective behaviour changes in response to the epidemic situation (as indicated). The gap in February 2022 is explained by a major app update. (b) The slowly varying relative transmissibility  $\langle T \rangle(t)$  (red) quantifying the intrinsic efficiency of SARS-CoV-2 transmission, measured from the ratio of reproduction numbers ( $R_{eff}$ ) and contact levels ( $CX$ ), see Eq. (1). The gray-shaded time interval is wild-type dominated and was used to calibrate  $CX$  from our crowdsourcing method and  $R_{eff}$  from infection surveillance (Figure S1(a, inset)). The rising frequencies of key SARS-CoV-2 immune escape variants (colored lines, see legend) and well as of vaccine status in Germany (light gray lines) are shown (right axis). (c) Comparison of SARS-CoV-2 effective reproduction numbers  $R_{eff}$  from infection surveillance (gray) and projected  $R_{true}$  using Eq. (2) (red). All reproduction numbers are assigned to their day of recording.

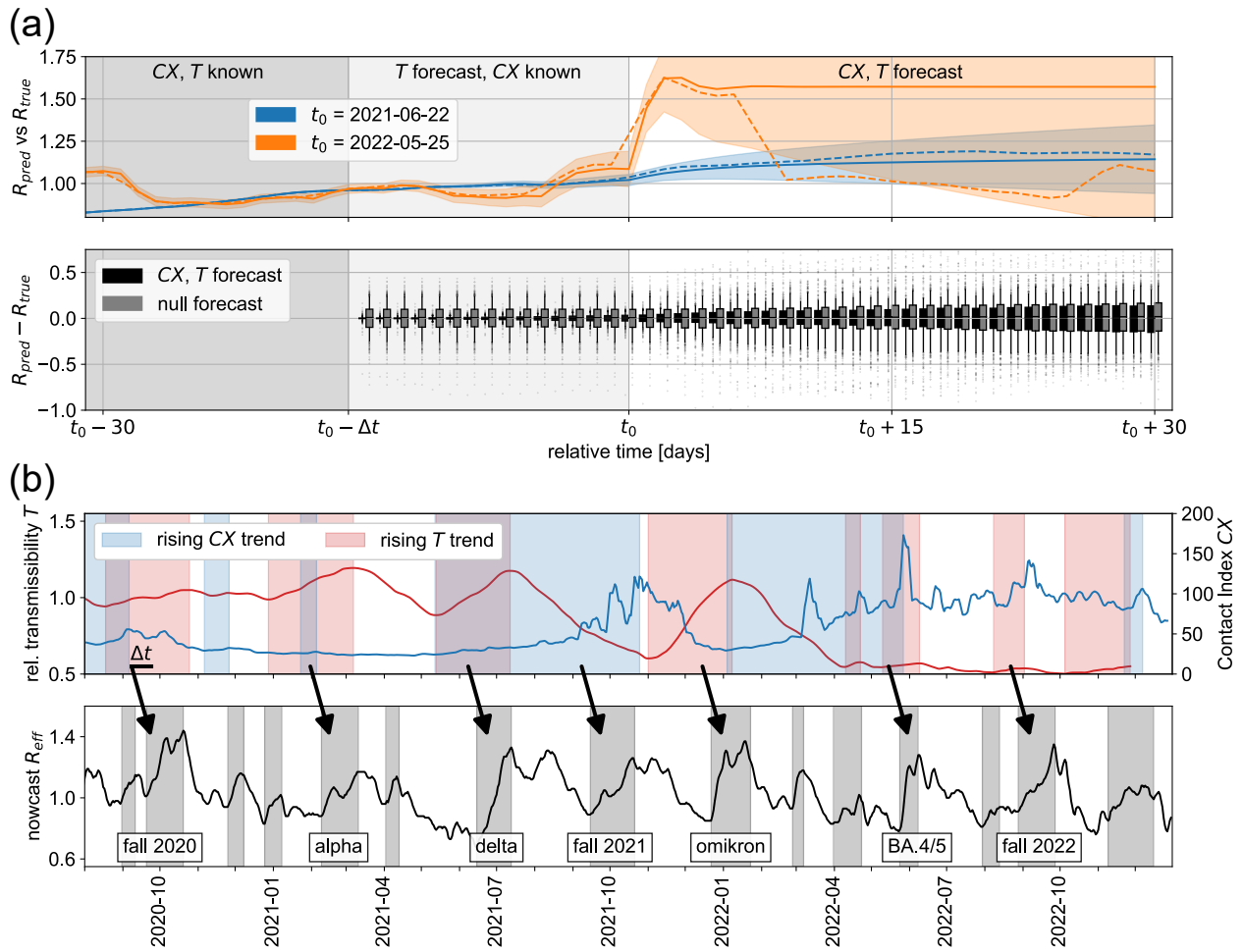


Figure 2: **Forecast of reproduction numbers and trends from contact and transmission efficiency levels.** (a, **upper panel**) Forecast  $R_{pred}$  of current and future SARS-CoV-2 reproduction numbers and their uncertainties (solid lines and shaded bands, respectively) using Eq. (2) and the  $CX$  and  $\langle T \rangle$  time series. Comparison with actual  $R_{true}$  values (dashed lines). Denoting the current day by  $t_0$ ,  $R_{eff}$  and  $\langle T \rangle$  are available up to  $t_0 - \Delta t$ , while  $CX$  is near real-time (available up to  $t_0$ ); the time series are projected beyond their last time points using ARIMA models. The forecast is shown for different choices of the current day  $t_0$  (see legend). (a, **lower panel**) The distribution of residuals between forecasted  $R_{pred}$  and actual  $R_{true}$  values over all choices of  $t_0$  over the course of 2 years (black box plots). Comparison to residuals from null projections of  $R_{eff}$  that make no use of  $CX$  (gray box plots), i.e. simple ARIMA model-based projection of infection surveillance data. The boxes indicate quartiles, while whiskers cover 90% of the data. (b) Identification of rising trends in both contact levels and transmission efficiency (upper panel) and their relation to rising trends in  $R_{eff}$  (lower panel).